Developing a cell-bound detection system for the screening of oxidase activity using the fluorescent peroxide sensor roGFP2-Orp1

As Published: 10.1093/protein/gzaa019

Publisher: Oxford University Press (OUP)

Persistent URL: https://hdl.handle.net/1721.1/134188

Version: Final published version: final published article, as it appeared in a journal, conference proceedings, or other formally published context

peds
protein engineering design & selection

Protein Engineering, Design and Selection, 2020, vol. 33, pp. 1–9
doi: 10.1093/protein/gzaa019
Original Article

OXFORD

Original Article

Developing a cell-bound detection system for the screening of oxidase activity using the fluorescent peroxide sensor roGFP2-Orp1

P.L. Herzog[1], E. Borghi[2], M.W. Traxlmayr[3], C. Obinger[3], H.D. Sikes[4], and C.K. Peterbauer[1,*]

[1]Food Biotechnology Laboratory, Department of Food Science and Technology, BOKU – University of Natural Resources and Life Sciences, Muthgasse 11, 1190 Vienna, Austria, [2]Department of Life Sciences, University of Modena and Reggio Emilia, Via Giuseppe Campi 287, 41124 Modena, Italy, [3]Institute of Biochemistry, Department of Chemistry, BOKU – University of Natural Resources and Life Sciences, Muthgasse 18, 1190 Vienna, Austria, and [4]Department of Chemical Engineering, MIT – Massachusetts Institute of Technology, 77 Massachusetts Avenue, Cambridge 02139, MA, USA

*To whom correspondence should be addressed. E-mail: clemens.peterbauer@boku.ac.at

Received 19 February 2020; Revised 2 June 2020; Accepted 8 July 2020

Abstract

Accurate yet efficient high-throughput screenings have emerged as essential technology for enzyme engineering via directed evolution. Modern high-throughput screening platforms for oxidoreductases are commonly assisted by technologies such as surface display and rely on emulsification techniques to facilitate single-cell analysis via fluorescence-activated cell sorting. Empowered by the dramatically increased throughput, the screening of significantly larger sequence spaces in acceptable time frames is achieved but usually comes at the cost of restricted applicability. In this work, we tackle this problem by utilizing roGFP2-Orp1 as a fluorescent one-component detection system for enzymatic H_2O_2 formation. We determined the kinetic parameters of the roGFP2-Orp1 reaction with H_2O_2 and established an efficient immobilization technique for the sensor on *Saccharomyces cerevisiae* cells employing the lectin Concanavalin A. This allowed to realize a peroxide-sensing shell on enzyme-displaying cells, a system that was successfully employed to screen for H_2O_2 formation of enzyme variants in a whole-cell setting.

Key words: enzyme, flow cytometry, H_2O_2, screening, surface display

Introduction

During the past decades, many enzymes have emerged to complement conventional chemical processes in various industries. Their utilization as highly specific and tunable biocatalysts has accelerated the expansion of novel biocatalytic processes and technology. The demand for improved catalytic properties, increased stability under process conditions and for non-native reactions has led to the establishment of a wide array of enzyme engineering techniques, including directed evolution (Chen and Arnold, 1991; Kuchner and Arnold, 1997; Renata *et al*., 2015). Directed evolution experiments generally require a balanced and sufficiently large library of variants accompanied by a screening method that reliably maintains the connection of genotype and phenotype (Fischlechner *et al*., 2014) and allows sufficient throughput (Porter *et al*., 2016; Truppo, 2017). Display methods immobilizing proteins on the surface of phage particles (Smith and Petrenko, 1997) and yeast cells (Boder and Wittrup, 1997) have greatly boosted the development of screening technologies for the engineering and evolution of, e.g. antibodies, where the assay simply involves binding to a labeled antigen.

Catalytic screening assays for enzymes, oxidoreductases in particular, are a different proposition due to the diffusible nature of enzyme substrates, cofactors and products. This generally demands some form of compartmentalization, e.g. in microtiter plates, which in turn limits throughput due to the practical demands of handling large

numbers of plates: bench space, manipulation, reagent distribution, readout, time. Practically, the screening of 10^4–10^5 variants per month appears to be a limit, even when using automated handling stations, as described in literature (Dörr *et al*., 2016). One approach to overcome this problem is through further miniaturization, by distributing enzyme variant producing cells and reaction components in emulsion droplets (water-in-oil, water-in-oil-in-water) or hydrogels to create microcompartments (Aharoni *et al*., 2005; Ostafe *et al*., 2014; Pitzler *et al*., 2014; Blažić *et al*., 2019; Vanella et al. 2019a; Markel *et al*., 2020). These droplets establish a reaction chamber for—statistically—single enzyme variants and can be analyzed via fluorescence activated cell sorting (FACS). This allows the screening of dramatically larger libraries and provides access to a larger sequence space with reasonable effort in shorter times, with throughputs in the range of 10^5 library variants within days reported for different oxidoreductases (Ostafe *et al*., 2014; Zhu *et al*., 2015; Ilić Đurđić *et al*., 2020). Several limitations remain: the water–oil interface maintains the reactants within the droplets and prevents influx into the system, therefore all assay components (substrate, secondary enzyme, fluorescent signal molecules) have to be supplied together with the enzyme-producing cells at emulsification. Appropriate distribution of cells into droplets needs to be optimized, and enzyme production and reaction start may vary across droplet populations. Increasing efforts are therefore directed toward systems that make artificial compartmentalization obsolete by physically linking a detectable readout of enzyme activity to the enzyme-producing cell harboring the respective variant gene. Most examples utilize a secondary enzyme like a peroxidase and some form of radical-mediated polymerization of a detectable (fluorescent) signal molecule to the cell (Lipovšek *et al*., 2007; Ostafe *et al*., 2014; Pitzler *et al*., 2014; Blažić *et al*., 2019; Ilić Đurđić *et al*., 2020). With the exception of the hydrogel-polymerization-based approach by Vanella *et al*. (Vanella *et al*., 2019b; Vanella *et al*. 2019a), none of these approaches, while successful in principle, could entirely obviate artificial compartmentalization. roGFP2-Orp1 is an artificial combination of a redox sensitive GFP variant (roGFP2) fused to the H_2O_2 sensing peroxidase Orp1—synonymously Gpx3 or Hyr1 (Ma *et al*., 2007)—and has been established as a genetically encoded fluorescent peroxide sensor by T. Dick *et al*. in 2009 (Gutscher *et al*., 2009). The mode of action of roGFP2-Orp1 is governed by a catalytic cysteine in Orp1. Upon contact with H_2O_2, Orp1 mediates the formation of a disulfide bridge on the adjoining roGFP2 moiety which results in a modified fluorescence spectrum of the fluorescent protein. These changes are most prominent at around 400 nm and 490 nm excitation and hence a fluorescence intensity ratio of 400/490 nm excitation at 520 nm emission (or similar) is commonly used to indicate the redox change in roGFP2-based sensors. In 2017, a comprehensive analysis of the roGFP2-Orp1 reactivities with relevant oxidant species was carried out and concluded that the sensor does not exclusively respond to H_2O_2 (Müller *et al*., 2017). Although roGFP2-Orp1 is robustly specific in a physiological (*in vivo*) setting, a pronounced unspecific reactivity in the presence of ambient oxygen concentrations was highlighted in this *in vitro* study.

In this work, we aimed to adapt roGFP2-Orp1 as a screening tool for H_2O_2-producing oxidases and dehydrogenases fit for whole-cell high-throughput screenings. We defined the performance parameters of roGFP2-Orp1 as a fluorescent sensor to (relatively) quantify enzymatic H_2O_2 production. We were able to apply this concept to distinguish between varying H_2O_2 formation rates using roGFP2-Orp1 in combination with soluble pyranose 2-oxidase or surface-displayed cellobiose dehydrogenase (CDH) variants. We then explored the coimmobilization of recombinantly produced roGFP2-Orp1 on the surface of yeast cells displaying a H_2O_2-producing enzyme, thus providing an artificial shell for local H_2O_2 detection that can be employed for whole-cell screening of cells producing enzyme variants in a high-throughput setting without artificial compartmentalization.

Results

Production and purification of roGFP2-Orp1

Escherichia coli (*E. coli*) NEB Express I^q cells, harboring the His-tagged roGFP2-Orp1 gene downstream of a T5 promoter, were cultivated in a shaking flask fermentation of 1.5 L. With this, 22 g of intensely green-colored *E. coli* cell pellet could be produced. After cell disruption and immobilized metal affinity chromatography (IMAC), the presence of the roGFP2-Orp1 protein was visible in various fractions by its characteristic fluorescence and a band at ∼50 kDa in SDS PAGE (Fig. S1), conforming to the protein's 49.1 kDa theoretical size. An additional purification step with size exclusion chromatography (SEC) yielded 164 mg of apparently pure protein. The identity of the purified full-length roGFP2-Orp1 was confirmed by peptide mapping via mass spectrometry.

Determination of kinetic parameters for the reaction of soluble roGFP2-Orp1 with H_2O_2

In order to quantify the formation of oxidized roGFP2-Orp1 during the sensor's reaction with H_2O_2 by means of fluorescence, it was necessary to determine the absolute change in fluorescence signals between the reduced and oxidized state and relate it to a molar amount of roGFP2-Orp1. This we accomplished by assessing fluorescence signals between a reduced (dithiothreitol, DTT incubation) and an oxidized (H_2O_2 incubation) reference state at 400 versus 490 nm excitation and 520 nm emission, respectively. The calculations allowed to estimate differential molar fluorescence extinction coefficients (ε_{ox}) for the oxidation reaction and yielded $\varepsilon_{ox,490}$ = −93 209 arbitrary units (a.u.) μM^{-1} at 490 nm and $\varepsilon_{ox,400}$ = 25 449 a.u. μM^{-1} at 400 nm (Fig. S2). It should be noted that these fluorescence coefficients only apply for the given experimental setup and detection settings. This is due to the fact that the detection of fluorescence signals, contrary to absorbance, depends on laser and detector gain settings and is not an absolute measurement. Aided by the estimated $\varepsilon_{ox,490}$ at 490 nm excitation, which was preferred for calculations due to the comparably higher signal, reactions of purified roGFP2-Orp1 with H_2O_2 allowed to estimate apparent kinetic parameters: a K_m of 0.30 ± 0.04 µM, V_{max} of 0.09 ± 0.01 µM min^{-1} was determined and yields a k_{cat} of 0.11 ± 0.01 min^{-1} at 0.9 µM sensor concentration (Fig. S3). As these kinetic parameters reflect the reaction cascade of the whole entirety of roGFP2-Orp1 they are not representative for the potentially much faster reaction rates of the Orp1 moiety with H_2O_2.

Reactions of roGFP2-Orp1 with soluble pyranose 2-oxidase

Purified roGFP2-Orp1 was utilized in combination with pyranose 2-oxidase (POx), a pronounced oxidase, to resolve varying peroxide production rates by the enzyme. In this experimental setup, POx and roGFP2-Orp1 were present at a stoichiometric ratio of 1:100 and the POx oxygen-to-peroxide turnover was fueled with varying concentrations of D-glucose, the preferred substrate for the enzyme. This resulted in substrate-dependent rates of H_2O_2 formation that were

traced via the roGFP2-Orp1 fluorescence until all sensor molecules were oxidized. The apparent slopes (Fig. 2A) display a saturation of reaction rates at a D-glucose concentration of ~250 µM. These results are in accordance with published kinetic data on POx which, dependent on the testing conditions, reports a D-glucose concentration at half maximal reaction rate (*Km*) in the triple digit µM range as was previously reported (Leitner, Volc and Haltrich, 2001; Tasca *et al.*, 2007; Salaheddin *et al.*, 2009; Spadiut *et al.*, 2009; Brugger *et al.*, 2014a; Halada *et al.*, 2016).

A similar differentiation of hydrogen peroxide production rates was obtained when different sugar substrates, to which POx has varying substrate specificity, were used at constant concentrations. In these reactions, D-glucose and D-xylose are preferred over D-galactose and D-maltose as substrates and yield steeper signal increases. No reaction was observed for D-fructose, D-glucose-1-phosphate and D-mannose (Fig. S4), in agreement with data from literature (Leitner *et al.*, 2001).

To simulate the behavior of roGFP2-Orp1 in a screening of oxidase variants, we repeated the experimental setup employing a constant D-glucose concentration in combination with established POx variants, all exhibiting an altered kinetic profile for oxygen and thus varying in their hydrogen peroxide formation rate (Brugger *et al.*, 2014b). As is observable in Fig. 2B, variants with a reportedly diminished oxidase activity: L547R, Q448H, N593C and the combined variant T166R/N593C could be discriminated from the *wt* due to their decreased H_2O_2 formation rate. Variant T166R expectedly aligns with the *wt* whereas also L545C display a reaction curve similar to the *wt* despite its decreased turnover rate for oxygen. To back literature-derived data, we assessed the variants different H_2O_2 formation rates utilizing the Amplex Red/peroxidase assay under the same experimental conditions as in the roGFP2-Orp1 setup: relative activities are given in brackets in the graph.

The saturation effect observed for the *wt* and variants T166R, L545C could be due to a limitation in the resolving power of the roGFP2-Orp1 sensor, that—present at a molar excess of 100:1—operates above a certain threshold of H_2O_2 production it is not able to process. As can be seen in Figs 2 and 3, negative controls (blank) without substrate also show a distinct increase in the fluorescence ratio, most likely from unspecific oxidation of the roGFP2-Orp1 sensor in the presence of ambient oxygen, as was described previously (Müller *et al.*, 2017). As was examined, this degree of unspecific oxidation of the roGFP2-Orp1 sensor disproportionally increases with lower concentrations (Fig. S5).

Reactions of soluble roGFP2-Orp1 with displayed CDH

We efficiently displayed *Myriococcum thermophilum* (synonymously *Crassicarpon hotsonii*) CDH flavin domain *wt* (CDH-F) and the oxygen reactive variant N748G (Kracher *et al.*, 2019) (CDH-F+) on the surface of *Saccharomyces cerevisiae (S. cerevisiae)* cells using the established Aga2 yeast surface display system (Boder and Wittrup, 1997; Angelini *et al.*, 2015). Display levels and enzyme activity were well-correlated and highest specific activities were obtained between 24 and 38 hours induction at 20°C. For CDH-F+ apparent oxidase activities of 1.7—2.8 mU $ODml^{-1}$ were reached, where 1 mU $ODml^{-1}$ is defined as the formation of 1 nmol of H_2O_2 per minute per milliliter of cell suspension of an OD_{600} 1.0. For CDH-F and the empty vector control (EVC), no peroxide formation above the background was detected. Both CDH variants are displayed at near identical levels (Fig. S6).

Freshly induced, washed cells were incubated with purified roGFP2-Orp1 and equilibrated for 100 seconds before cellobiose was added (Fig. 3). As was expected, a H_2O_2-mediated increase in the roGFP2-Orp1 fluorescence ratio was only detected for the displayed oxygen reactive CDH-F+ variant; CDH-F did not show any substrate specific H_2O_2 production above the background (EVC), which was also confirmed using the Amplex Red/peroxidase assay (Fig. S7). After the reaction had proceeded for another 420 seconds, iodoacetamide (IAA)—a well-established alkylating reagent for cysteines—was added to arrest the remaining unreacted roGFP2-Orp1 in the reduced state. Presumably, IAA derivatizes the cysteine thiol form and hence can prevent the formation of the cysteine disulfide bond and the concomitant shift in the fluorescent signatures in the roGFP2 moiety. For the untreated samples, the reactions proceeded as projected. Again, an increase in the fluorescence ratio was observed for the control reactions. Strikingly, this background reaction was also stopped by IAA. IAA thus functions as a potent stop reagent for the assay reaction and could be used in the format of a whole-cell assay in a one-pot screening reaction to stop the parallel unspecific reactions prior to analysis via flow cytometry and cell sorting.

Biotinylation and immobilization of roGFP2-Orp1 via the "ConAct" system

A sequence encoding an N-terminal 15 amino acid AviTag was added to the roGFP2-Orp1 gene to facilitate *in vivo* biotinylation during expression in *E. coli*. Repeating the previously used production procedure for native roGFP2-Orp1, we could produce mg amounts of pure biotinylated roGFP2-Orp1. Analysis of the purified protein via mass spectrometry confirmed the presence of the full sequence and complete biotinylation, and assessment of purified biotin-roGFP2-Orp1 confirmed reaction kinetics comparable to the unbiotinylated protein (Fig. S8).

Concanavalin A (ConA) is a plant-derived lectin which specifically binds to high-mannose type glycosyl moieties, characterized by a single digit µM dissociation constant K_d (Coulibaly and Youan, 2014). Effective and specific immobilization of biotinylated roGFP2-Orp1 on the yeast cell wall was accomplished by binding biotinylated ConA on the yeast cell wall and combining it with streptavidin (which is a tetramer) to bridge the two biotinylated moieties (ConAct). As could be shown by flow cytometry (Fig. S9), only the mixture containing all components could facilitate efficient immobilization of biotin-roGFP2-Orp1. The ConAct system was preferred over click chemistry-based technology to capture proteins on the cell surface (Rhiel *et al.*, 2014) due to the exceptionally high binding capacity, reliability and ease of handling.

Trials of a whole-cell assay combining surface display of CDH with immobilized roGFP2-Orp1

ConA-biotin, streptavidin and reduced biotin-roGFP2-Orp1 were added sequentially to induced and washed cells displaying CDH-F or CDH-F+ to generate a space-proximity detection system (Fig. 1). Soluble roGFP2-Orp1 was added in excess to the reaction mix to buffer unspecific oxidation at the cell surface. We then assessed whether this system is capable of differentiating the peroxide production of displayed CDH-F+ in comparison to CDH-F (negative) when the assay reactions were started with the native CDH substrate cellobiose (Fig. 4). With proceeding reaction time, differences in the ratio of fluorescence intensities were detectable as CDH-F+ fluorescence

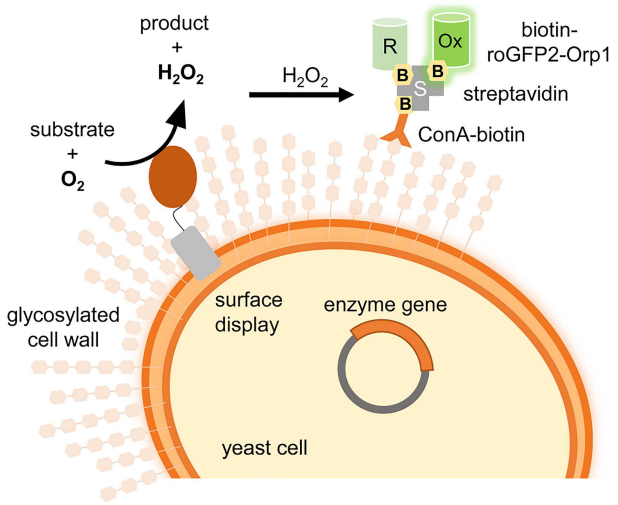

Fig. 1 Whole cell screening assay for peroxide formation with immobilized roGFP2-Orp1. Scheme depicting the designed whole cell screening assay where the displayed enzyme oxidizes its substrate and concomitantly reduces oxygen to H_2O_2. The formed H_2O_2 causes oxidation of neighboring biotin-roGFP2-Orp1 from the reduced (R) to the oxidized (Ox) state and is connected to a change in the fluorescence. roGFP2-Orp1 is in close proximity since it is also immobilized on the surface of the cell via the ConA-biotin, streptavidin ConAct system.

signals at 405 nm excitation increased while the prospected negative reaction of CDH-F maintained a reduced state with predominant 488 nm excitation. For CDH-F, gated events reached a level of not <4.54% of the overall population (20 min) whereas for CDH-F+ the gated event count increased from 6.90% (1 min) to 41.08% (20 min), 9-fold of the respective CDH-F sample at stopping time and clear sign for specific roGFP2-Orp1 oxidation. To confirm specific enzymatic activities after the immobilization procedure we evaluated the prepared cultures with the established Amplex Red/Peroxidase assay and detected minor impact of washing and staining steps on the activity (65% remaining activity) of the displayed CDH variants and no unspecific H_2O_2 production. The immobilized biotin-roGFP2-Orp1 virtual concentration used is ~0.08 µM and thus around 8% of the previously used soluble roGFP2-Orp1 concentration in the assays.

Discussion

With this report, we provide a mechanistic analysis of roGFP2-Orp1 as a fluorescent H_2O_2 resolving reporter and propose potential applications for screening of hydrogen peroxide producing enzymes. The characterization of its fundamental kinetic parameters and reactivities are valuable in all fields of application, for the improved understanding of this and other fluorescent probes and for the development of novel screening technologies.

roGFP2-Orp1 is a sensitive H_2O_2 reporter with a relatively low reaction rate

With the assessment of fluorescent intensities of roGFP2-Orp1 at the fully reduced and oxidized endpoint we were able to correlate the change in fluorescence signals to the roGFP2-Orp1 concentration and use it for the estimation of kinetic parameters K_m and V_{max} (Fig. S3). With the given experimental setup, we could estimate a K_m of 0.3 µM, suggesting a pronounced specificity for the interaction of roGFP2-Orp1 with H_2O_2. The estimation of V_{max} allowed to calculate a catalytic rate constant k_{cat} of 0.11 min^{-1}, a comparably slow turnover of hydrogen peroxide when compared to the reactions of thiol peroxidases homologous to Orp1 (Parsonage *et al.*, 2005; Tanaka, Izawa and Inoue, 2005). Most likely, the rate limiting step in its fluorescent response to H_2O_2 is the non-native interdomain thiol-disulfide exchange from the Orp1 to the roGFP2 moiety, a mechanism that is likely defined by the probability for close contact of this non-native couple of domains.

The roGFP2-Orp1 resolving power depends on its stoichiometric excess

When combining the roGFP2-Orp1 peroxide sensor with H_2O_2 producing enzymes, one needs to acknowledge the sensor's relatively low turnover number of around 0.1 min^{-1}. This is of importance when hydrogen peroxide is produced at substantially higher rates as was observed in our experiments when H_2O_2 formation by POx was detected with roGFP2-Orp1 at a molar excess of a 100-fold (Fig. 2A and B). POx *wt* and variants T166R, L545C are pronounced oxidases with reported catalytic constants k_{cat} for H_2O_2 formation of 42 s^{-1}, 11 s^{-1} and 2.7 s^{-1}, respectively (Brugger *et al.*, 2014a). At the given conditions, the roGFP2-Orp1 sensor could not resolve these large differences in hydrogen peroxide formation since its turnover rates could not keep pace with elevated production. However, the fluorescent probe was successfully used to identify H_2O_2 formation from variant N593C (Brugger *et al.*, 2016), a rather strict dehydrogenase with substantially reduced oxygen reactivity (0.18 s^{-1}), which underlines the exceptional sensitivity of roGFP2-Orp1.

roGFP2-Orp1 is susceptible to unspecific oxidation reactions

The reactivity of roGFP2-Orp1 with molecular oxygen and various radical species has been extensively analyzed by Müller et al., who concluded the Orp1 moiety to be more susceptible to unspecific thiol oxidation under aerobic conditions. Whether this is a direct effect of molecular oxygen or a radical-mediated oxidation, potentially from Fenton-like chemistry by transition metals in the buffer, was not resolved in their work (Müller *et al.*, 2017). Our experiments with roGFP2-Orp1 *in vitro* confirmed that specific reactions of the probe with H_2O_2 can only be achieved in the presence of ion-complexing EDTA (Fig. S10). In our experiments at ambient oxygen concentrations (Figs 2, 3, S4, S5), a certain degree of unspecific oxidation is detected in negative controls and blank measurements even though freshly degassed buffers were used. Especially the data summarized in Fig. S5 points toward a more unfavorable ratio of ambient oxygen to roGFP2-Orp1 with lower sensor concentrations.

Utilization of roGFP2-Orp1 in whole-cell assays

The first report on the employment of a fluorescent H_2O_2 probe for the screening of enzyme activity describes an intracellular system. The synthetic fluorescent H_2O_2 sensor HyPer was used for the detection of H_2O_2 formed by the uncoupling reaction of cytochrome P450 (Lim and Sikes, 2015) in the *E. coli* cytosol. In our setup, the enzyme (CDH variants) is displayed on the cell surface since this simplifies the addition of substrates and allows quantification of expression levels and normalization of activities via staining of a suitable tag with fluorescently labeled antitag antibodies if desired. Immobilization of roGFP2-Orp1—mediated by the ConAct system—in close spatial

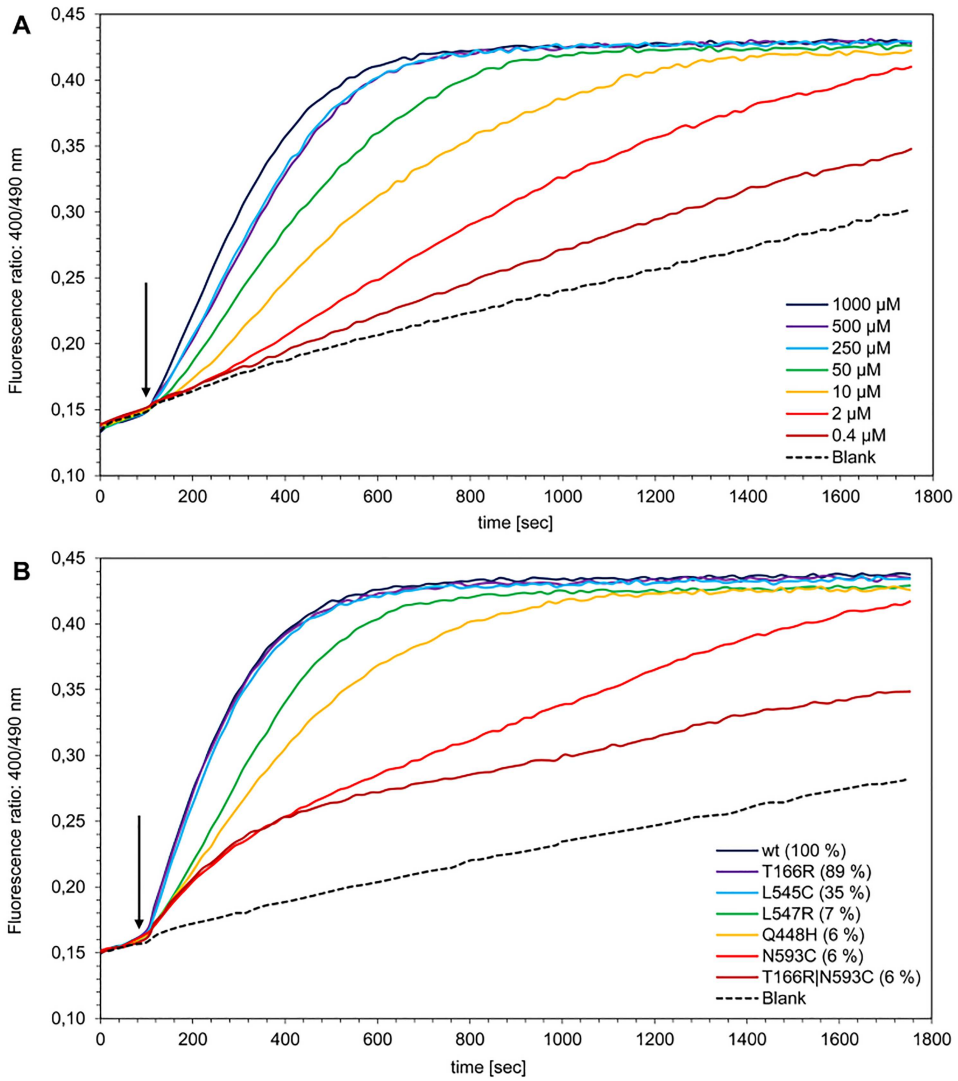

Fig. 2 Detection of pyranose 2-oxidase (soluble) dependent H_2O_2 formation with roGFP2-Orp1 (soluble). About 1.0 µM roGFP2-Orp1 was mixed with 0.01 µM recombinant POx from *T. ochracea* and let equilibrate for 100 seconds before substrate was added to start H_2O_2 formation (arrow). (A) POx wt was fueled with d-glucose at concentrations of 0.4 µM, 2 µM, 10 µM, 50 µM, 250 µM, 500 µM, 1000 µM and buffer only (dotted). (B) POx variants: wt, T166R, L545C, L547R, Q448H, N593C and the combinational variant T166R|N593C were fueled with d-glucose at a concentration of 500 µM. Numbers in brackets reflect relative activities that were determined with the established Amplex Red/peroxidase assay under identical experimental conditions. Fluorescent intensities were tracked for 1800 seconds.

proximity to the place of H_2O_2 formation (the oxidase) (Fig. 1) minimizes crosstalk between neighboring cells in a reaction mix without compartmentalization in emulsions (Aharoni *et al.*, 2005; Ostafe *et al.*, 2014). The reactions can be stopped with IAA (Fig. 3) before cells are analyzed for their 400/490 nm fluorescence ratio and separated using FACS.

We used this system to successfully differentiate between CDH variants with differing oxidase activities. As enzymatic reactions progressed, cell populations shifted in their 405 versus 488 nm fluorescence excitation ratio due to H_2O_2-mediated roGFP2-Orp1 oxidation and could be gated against the negative control (Fig. 4). It is still observable though, that populations are not strictly homogeneous and especially scattered for CDH-F+ in early reactions which could stem from a small portion of false-positives or an unsynchronized reaction start.

In our trials, differentiation of variants could only be accomplished when soluble roGFP2-Orp1 was added in excess to the assay reactions to buffer unspecific oxidation of the immobilized biotin-roGFP2-Orp1 by ambient oxygen. As was pointed out, higher roGFP2-Orp1 concentrations were less susceptible to unspecific oxidation (Fig. S5). Consequently, reactions could only be resolved via flow cytometry after cells and immobilized sensor were separated from the reaction mix via centrifugation. In the absence of excess roGFP2-Orp1, positive and negative reactions were indifferentiable since the unspecific oxidation left little margin for the contribution of peroxide-mediated oxidation (Fig. S11).

ALthough the screening assay employing roGFP2-Orp1 could benefit from an air-free environment to minimize disturbances—reactions could be performed in a 'glove box'—the formation of H_2O_2 by the screened enzyme is dependent on (low concentrations

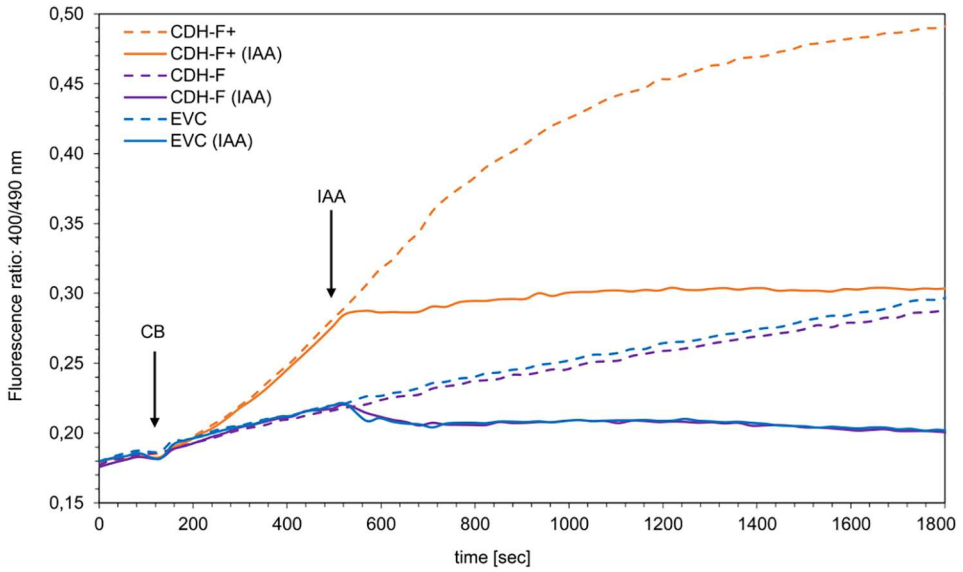

Fig. 3 Detection of cellobiose dehydrogenase-dependent (yeast-displayed) H_2O_2 formation with soluble roGFP2-Orp1 in a whole cell format. About 1.0 μM roGFP2-Orp1 was mixed with CDH-displaying *S. cerevisiae* cells present at an optical density OD600 of 1.0 and let equilibrate for 100 seconds before cellobiose was added to start the reaction (CB, arrow). Fluorescence ratios were tracked for the oxygen-reactive CDH-F+ variant (orange), the CDH-F wild type (violet) and an empty vector control (EVC) (blue). Four hundred and twenty seconds into the reaction, 50 mM IAA was added (IAA, arrow) to the samples (full lines). Negative controls (dashed lines) was added CB but buffer instead of IAA.

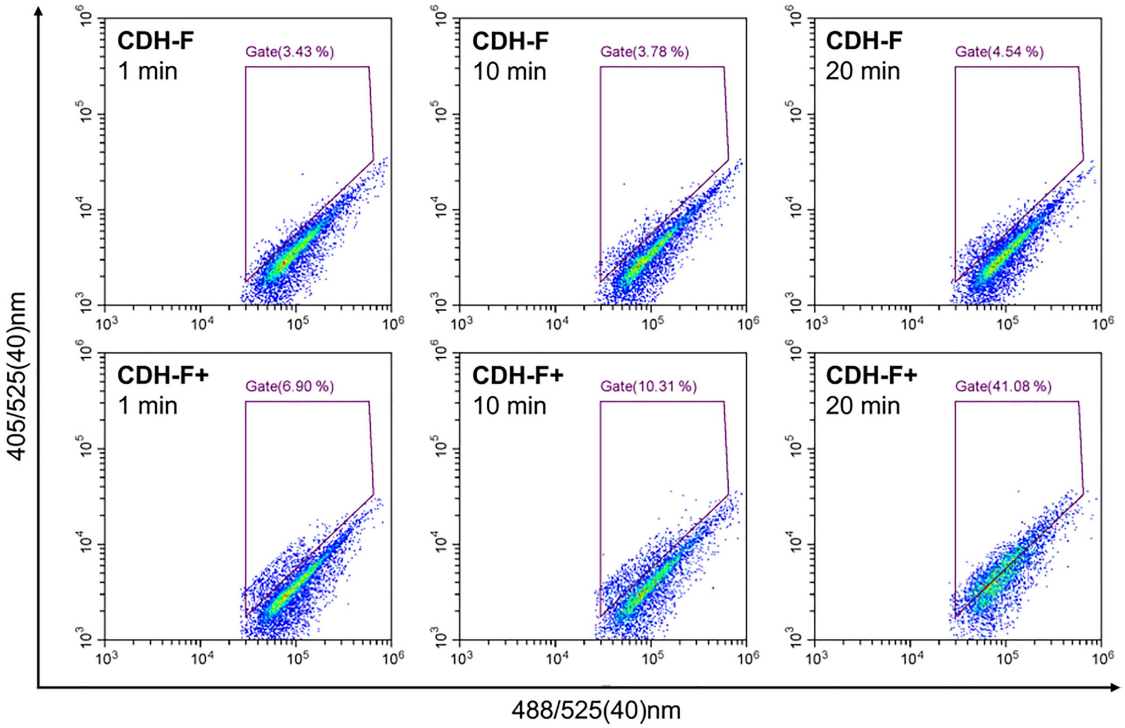

Fig. 4 Whole cell assay for the detection of displayed CDH-F+ activity with immobilized roGFP2-Orp1. *S. cerevisiae* cells displaying CDH-F or CDH-F+, respectively, were stained with ConA-biotin, streptavidin and biotin-roGFP2-Orp1 to immobilize the biotinylated sensor protein on the surface of the yeast cells. With the addition of the cellobiose substrate the formation of H_2O_2 was initiated in the case of CDH-F+. Accumulation of peroxide then led to oxidation of the roGFP2-Orp1 on the surface of individual cells which could be tracked by the fluorescence ratio. Reactions were stopped with IAA after 1, 10 and 20 minutes. Cells were washed and analyzed in the flow cytometer at 405/525(40) nm and 488/525(40) nm. About 10 000 events were recorded and the gate placed according to the CDH-F negative control. Numbers in brackets represent the proportion of gated events.

of) oxygen, and total exclusion of oxygen is not an option. Decreased O_2 concentrations may also be beneficial, but the required equipment and handling procedures run counter to the idea of a user-friendly and simple high-throughput screening system.

Conclusion

In this report, we describe the development of a screening platform for oxidase activity employing roGFP2-Orp1 as a fluorescent peroxide sensor that does not require artificial compartmentalization. Analysis of its catalytic properties and insights from trials in soluble format allowed us to successfully employ this system in combination with cells displaying CDH variants. The major obstacle, unspecific reactivity of the sensor with molecular oxygen, could be overcome by applying an excess of soluble sensor.

For full adaptation to ultra-high-throughput screenings, a modified sensor performing faster with hydrogen peroxide is desirable. Ideally, a hydrogen peroxide-specific oxidation outperforming the unspecific oxidation to a significantly higher degree would widen the detectable activity ranges of enzymes of interest and make handling of the system more user-friendly. Future studies will evaluate the performance of this platform with large libraries of oxidase variants.

Material and Methods

Materials

Unless otherwise stated, all chemicals and reagents used in this study were of highest available purity and purchased from Sigma–Aldrich (Germany).

Recombinant expression and purification of roGFP2-Orp1

The pQE-60 roGFP2-Orp1 expression plasmid (Gutscher *et al.*, 2009), containing a C-terminal His-tag was kindly provided by Tobias Dick (Addgene plasmid #64976, RRID:Addgene_64976). After isolation, the purified plasmid was transformed into NEB Express I^q competent *E. coli* cells (New England Biolabs, Germany), its presence and identity were confirmed via sequencing (Microsynth AG, Austria). For recombinant protein production, *E. coli* cultures were routinely grown in TB medium, supplemented with 1.0 g L^{-1} glucose monohydrate and 100 µg ml^{-1} ampicillin. Expression and IMAC purification were carried according to a previously published protocol (Brugger *et al.*, 2014a) with the adaptation of inducing cultures at 20°C for 20 hours and using Tris HCl-based buffers at pH 8.0 for all cell disruption and purification steps. As a polishing step, active fractions were pooled and subjected to SEC using a 180 ml HiPrep Sephacryl SEC column (GE Life Sciences, Germany) with 50 mM Tris HCl, 500 mM NaCl pH 7.5. Clean and fluorescent chromatography fractions, as judged by SDS-PAGE and their fluorescence signal (isosbestic fluorescence Ex. 423 nm, Em. 520 nm) were pooled, desalted and concentrated with centrifugal filters before being stored at −80°C in freshly prepared storage buffer (10 mM Tris HCl, 5 mM EDTA, 1 mM DTT, 10% *w/w* glycerol, pH 7.5).

Protein analysis

The estimation of protein concentration was generally carried out by determination of the protein's absorbance at 280 nm wavelength. For His-tagged roGFP2-Orp1 an extinction coefficient of ε_{280} = 39 685 M^{-1} cm^{-1} was used. The presence of the full-length protein was confirmed via peptide mapping by LC–ESI–MS. The purity of purification fractions and pooled solutions was evaluated by SDS PAGE and carried out using precast stain-free gels (Bio-Rad, Austria) that were visualized spectroscopically.

Preparation of roGFP2-Orp1 for fluorescent measurements

Frozen stock solutions of roGFP2-Orp1 at about 200 µM were diluted to 9.0 µM in GFP buffer (100 mM potassium phosphate buffer, 5 mM EDTA, pH 7.25, degassed and saturated with nitrogen). To facilitate work with the redox probe, roGFP2-Orp1 solutions were initially reduced on ice for 20 minutes in GFP buffer containing 20 mM DTT. DTT concentration in the solution was gradually decreased to <10 µM by repeated rebuffering against GFP buffer in 0.5 ml, 50 kDa cut-off spin filters (Merck Millipore, Germany) (Gutscher *et al.*, 2009) before the solution was diluted to ∼1 µM and stored air-sealed for immediate use.

Unless otherwise stated, all measurements were carried out as 200 µl reactions in 96-well plate format. Fluorescent measurements were generally recorded at 400 nm, 490 nm excitation and 520 nm emission using an EnSpire alpha platreader (PerkinElmer, Austria). The resulting changes in fluorescence intensities at 520 nm, given in a.u., were commonly displayed as a ratio of 400 nm by 490 nm excitation, respectively and plotted against time.

Estimation of differential molar fluorescence extinction coefficients ε_{ox}

To quantify the correlation of roGFP2-Orp1 fluorescence and redox state, a dilution series (0.1–1.4 µM) of the fusion protein was equilibrated for 20 minutes in GFP buffer containing either 20 mM DTT or 0.1 mM H_2O_2. This yielded roGFP2-Orp1 in the reduced and oxidized state, respectively. Subsequently, fluorescence emission intensities (*IF*) at 400 nm, 490 nm excitation and 520 nm emission were recorded in 200 µl quintuplicates in a fluorescent plate reader and plotted against the roGFP2-Orp1 concentration. Obtained correlations, as linear least square fitted slopes (m), were used to calculate the change in fluorescence emission intensity per µM roGFP2-Orp1 (ε_{ox}) between the reduced and the oxidized state (oxidation reaction) at a certain wavelength (λ) for the given concentrations and experimental setup according to:

$$\varepsilon_{ox,\lambda} = m_{ox.,\lambda} - m_{red.,\lambda} = \frac{d\left(IF_{ox,\lambda}\right) - d\left(IF_{red,\lambda}\right)}{d\left([roGFP2 - Orp1]\right)} \qquad (1)$$

Based on the premise that every molecule of roGFP2-Orp1 can be present at only one of two distinct redox states, reduced or oxidized, the change in emission intensity for one molecule is proportional to the change in emission intensity of µM concentrations of roGFP2-Orp1. This principle was similarly described for the determination of roGFP redox potentials before (Aller, Rouhier and Meyer, 2013).

Determination of kinetic parameters of the H_2O_2-dependent roGFP2-Orp1 reaction

In order to estimate the kinetic parameters of the roGFP2-Orp1 reaction with H_2O_2, aliquots of the roGFP2-Orp1 fusion protein were prepared as described above and diluted to 1 µM in a 200 µl reaction mix. After an initial equilibration phase, H_2O_2 was added

in varying amounts to final concentrations of 0.05–10.0 µM. GFP buffer served as a blank measurement as described before (Gutscher *et al.*, 2009; Müller *et al.*, 2017). Resulting changes in the fluorescent signals were tracked for 1800 seconds and slopes obtained from four independent sets of measurements were calculated into catalytic rates using ε_{ox}. Apparent kinetic constants were estimated by nonlinear least-square regression fitting using the Microsoft Excel solver plugin.

Resolving enzymatic H_2O_2 formation with roGFP2-Orp1 *in vitro*

Initially, roGFP2-Orp1 was prepared as described before and diluted to 1 µM before being incubated with 10 nM of purified pyranose 2-oxidase (POx) from *Trametes ochracaea (*formerly *Trametes multicolor)*. To start the enzymatic formation of H_2O_2 by POx, D-glucose or alternative sugar substrates such as D-xylose, D-galactose, maltose were added after equilibration. For discrimination of activities of different POx variants, 10 nM of purified enzyme were used. Purified POx *wt* and variants were kindly gifted by Leander Sützl from BOKU University, Austria.

Display of CDH on the surface of *S. cerevisiae*

CDH from *Myriococcum thermophilum* (Zámocký *et al.*, 2008; Tan *et al.*, 2015), UniProtKB A9XK88 was expressed in a display format using the established yeast surface display format for *S. cerevisiae* (Boder and Wittrup, 1997; Angelini *et al.*, 2015). The gene sequence encoding the wild type flavin domain of CDH (CDH-F) and an engineered flavin domain with increased oxygen reactivity (CDH-F+) which was kindly provided by Prof. Roland Ludwig from BOKU University, Austria (Kracher *et al.*, 2019). The genes were cloned in frame into the pCTCON2 display plasmid, omitting the sequence encoding the 247 N-terminal residues comprising the signal peptide, cytochrome domain and linker. The recombinant constructs CDH-F, CDH-F+ and an EVC were transformed into competent *S. cerevisiae* EBY100 using the Frozen-EZ Yeast Transformation II Kit (Zymo Research, Germany). Vector and expression strain were kindly gifted by Dane Wittrup from MIT, USA.

Transformed cells were plated on SD-CAA selection plates and positive clones were expressed in SD-CAA liquid culture for 20 hours at 30°C prior to media change and induction in SG(R)-CAA medium supplemented with 1% *w/w* raffinose at 20°C for 30 hours (Puri *et al.*, 2013; Angelini *et al.*, 2015).

Assessment of display efficiency and enzyme activities

Assessment of display levels was carried out based on the fluorescent staining of a C-terminal myc-tag and detection by flow cytometry. The procedure consisted of binding of the myc-tag with an anti-myc (9B11) primary mouse antibody (Cell Signaling Technology, USA) and labeling of the primary antibody with an antimouse secondary antibody conjugated with fluorescent Alexa Fluor 647 dye (Cell Signaling Technology). In parallel, enzyme activities were evaluated by determining cellobiose dependent H_2O_2 formation by CDH-F+ using the established Amplex Red/peroxidase assay (10).

Use of roGFP2-Orp1 in combination with cell-displayed CDH

The CDH constructs were expressed as described. Cell suspensions were washed twice with phosphate buffered saline (PBS) at pH 7.4 to remove media components and diluted to an optical density (OD_{600}) of 5.0 in 100 mM potassium phosphate buffer, 5 mM EDTA at pH 6.0 (PPB, pH 6). In parallel, aliquots of roGFP2-Orp1 were prepared as described and diluted in GFP buffer. Aliquots of induced *S. cerevisiae* cultures displaying CDH-F, CDH-F+ and an EVC were transferred to a 96-well plate before roGFP2-Orp1 solution was added. After an initial equilibration phase of 100 seconds, enzymatic reactions were started with the addition of cellobiose to yield reaction mixtures of 1.0 µM roGFP2-Orp1, cells of OD_{600} = 1.0 and 10 mM cellobiose in 100 mM PPB pH 6.0. Another 420 seconds into the reaction IAA was added to a concentration of 50 mM. Fluorescent signals were tracked for 1800 seconds.

Immobilization of biotinylated roGFP2-Orp1 on yeast cells

We used a commercial *in vivo* biotinylation system, acquired from Avidity (USA), to equip roGFP2-Orp1 with an N-terminal AviTag. In this system, coexpression of the biotin ligase BirA mediates the enzymatic biotinylation at the AviTag during recombinant expression in *E. coli*. The roGFP2-Orp1 coding sequence was introduced in-frame into the pAN4 expression vector (Avidity) using the NEBuilder HiFi Assembly Kit (New England Biolabs). The correct assembly of the pAN4 biotin-roGFP2-Orp1 expression plasmid was confirmed by sequencing before the construct was transformed into competent *E. coli* EVB101 cells for expression. The production of N-terminally biotinylated roGFP2-Orp1 was carried out as recommended by the supplier with the difference of inducing protein expression at 20°C for 18 hours. Purification of biotin-roGFP2-Orp1 was carried out as described above.

For plant lectin ConA mediated immobilization of biotinylated roGFP2-Orp1 on *S. cerevisiae*, EBY100 cells were cultivated in SD-CAA medium, harvested and washed in PBS twice as described. Immobilization was done after incubating 1.0 ml cells of OD_{600} 1.0 in blocking buffer (PBS + 2% bovine serum albumin BSA) by consecutive incubation with 10 µg biotinylated ConA (Vector laboratories, USA), 50 µg Streptavidin (New England Biolabs) and 250 µg biotin-roGFP2-Orp1, each for 30 minutes shaking at room temperature. Between all steps, cells were washed with PBS-A (PBS + 0.1% BSA) by centrifugation at 12 000 rcf for 2 minutes and gentle resuspension. PBS-A was also used as a diluent for the labeling reagents. Labeled cells were analyzed in a CytoFLEX S flow cytometer (Beckman Coulter, USA) using a 488 nm laser for excitation and detection in the FITC channel (525/40 nm).

Detection of displayed CDH activities with cell-tethered roGFP2-Orp1

Biotin-roGFP2-Orp1 was reduced and prepared for fluorescent measurement as described for the unbiotinylated protein. *S. cerevisiae* cells were induced to display CDH-F and CDH-F+. From each clone, 500 µl cells of OD 1.0 were harvested, washed and blocked in blocking buffer. Subsequently, immobilization was carried out while maintaining biotin-roGFP2-Orp1 in the degassed buffer prior to use. About 25 µg ConA-biotin, 50 µg Streptavidin and 250 µg biotin-roGFP2-Orp1 were used for the sequential immobilization. For the whole cell assay reaction, cells were maintained in 2 ml of 125 µg ml^{-1} biotin-roGFP2-Orp1 during the course of the reaction to detect peroxide locally (immobilized sensor) but simultaneously buffer the oxygen dependent background reaction (soluble sensor). Reactions were started with 10 mM cellobiose and then sequentially stopped after 1, 5 and 20 minutes of reaction using 50 mM IAA.

The assay cell suspensions were then subjected to centrifugation at 12 000 rcf for 2 minutes and a subsequent washing step in PBS-A before being analyzed for fluorescent ratios in the flow cytometer with lasers operating at 405 and 488 nm in the FITC channel 525/40 nm.

Supplementary data

Supplementary data are available at *PEDS* online.

Acknowledgments

This work was supported by the Austrian Science Fund FWF through the Doctoral Program BioToP Biomolecular Technology of Proteins (FWF W 1224) and by the Erasmus+ EU program for education. Experimental analysis and data processing were supported by EQ-BOKU VIBT GmbH and the BOKU Core Facility for Biomolecular and Cellular Analysis.
We especially like to thank Dr Leander Sützl for providing purified pyranose 2-oxidase variants and Roland Ludwig for supplying us with an engineered cellobiose dehydrogenase variant.

Authors' Contribution

Dr Florian Hollfelder, PEDS Board Member edited the manuscript.

Conflict of Interest

None declared.

References

Aharoni, A., Amitai, G., Bernath, K. *et al.* (2005) *Chem. Biol. Cell Press*, **12**, 1281–1289. doi: 10.1016/J.CHEMBIOL.2005.09.012.

Aller, I., Rouhier, N. and Meyer, A.J. (2013) *Front. Plant Sci.*, **4**, 1–12. doi: 10.3389/fpls.2013.00506.

Angelini, A., Chen, T.F., de Picciotto, S. *et al.* (2015) Protein engineering and selection using yeast surface display. In Yeast Surface Display. Humana Press, New York, NY, pp. 3–36.

Blažić, M., Balaž, A.M., Prodanovic, O. *et al.* (2019) *Appl. Sci.*, **9**, 1413. doi: 10.3390/app9071413.

Boder, E.T. and Wittrup, K.D. (1997) *Nat. Biotechnol.*, **15**, 553–557. doi: 10.1038/nbt0697-553.

Brugger, D. *et al.* (2014a) *PLoS One*, **9**, e109242–e109242. doi: 10.1371/journal.pone.0109242.

Brugger, D. *et al.* (2014b) *Biotechnol. J.*, **9**, 474–482. doi: 10.1002/biot.201300336.

Brugger, D., Sützl, L., Zahma, K. *et al.* (2016) *Phys. Chem. Chem. Phys.*, **18**, 32072–32077. doi: 10.1039/C6CP06009A.

Chen, K. and Arnold, F.H. (1991) *Biotechnology*, **9**, 1073–1077. doi: 10.1038/nbt1191-1073.

Coulibaly, F.S. and Youan, B.B.C. (2014) *Biosens. Bioelectron.*, **59**, 404–411. doi: 10.1016/j.bios.2014.03.040.

Dörr, M., Fibinger, M.P., Last, D. *et al.* (2016) *Biotechnol. Bioeng.*, **113**, 1421–1432. doi: 10.1002/bit.25925.

Đurdic, K.I., Ece, S., Ostafe, R. *et al.* (2020) *J. Biosci. Bioeng.* doi: 10.1016/j.jbiosc.2019.12.009.

Fischlechner, M., Schaerli, Y., Mohamed, M. *et al.* (2014) *Nat. Chem.*, **6**, 791. doi: 10.1038/nchem.1996.

Gutscher, M., Sobotta, M.C., Wabnitz, G.H. *et al.* (2009) *J. Biol. Chem.*, **284**, 31532–31540. doi: 10.1074/jbc.M109.059246.

Halada, P., Brugger, D., Volc, J. *et al.* (2016) *PloS One*, **11**, e0148108. doi: 10.1371/journal.pone.0148108.

Kracher, D., Forsberg, Z., Bissaro, B. *et al.* (2019) *FEBS J.*, febs.15067. doi: 10.1111/febs.15067.

Kuchner, O. and Arnold, F.H. (1997) *Trends Biotechnol.*, **15**, 523–530. doi: 10.1016/S0167-7799(97)01138-4.

Leitner, C., Volc, J. and Haltrich, D. (2001) *Appl. Environ. Microbiol.*, **67**, 3636–3644. doi: 10.1128/AEM.67.8.3636.

Lim, J.B. and Sikes, H.D. (2015) *Protein Eng. Des. Sel.*, **28**, 79–83. doi: 10.1093/protein/gzv003.

Lipovšek, D., Antipov, E., Armstrong, K.A. *et al.* (2007) *Chem. Biol.*, **14**, 1176–1185. doi: 10.1016/j.chembiol.2007.09.008.

Ma, L.H., Takanishi, C.L. and Wood, M.J. (2007) *J. Biol. Chem.*, **282**, 31429–31436. doi: 10.1074/jbc.M705953200.

Markel, U., Essani, K.D., Besirlioglu, V. *et al.* (2020) *Chem. Soc. Rev.*, **49**, 233–262. doi: 10.1039/C8CS00981C.

Müller, A., Schneider, J.F., Degrossoli, A. *et al.* (2017) *Free Radic. Biol. Med.*, **106**, 329–338. doi: 10.1016/J.FREERADBIOMED.2017.02.044.

Ostafe, R., Prodanovic, R., Nazor, J. *et al.* (2014) *Chem. Biol.*, **21**, 414–421. doi: 10.1016/j.chembiol.2014.01.010.

Parsonage, D., Youngblood, D.S., Sarma, G.N. *et al.* (2005) *Biochemistry*, **44**, 10583–10592. doi: 10.1021/bi050448i.

Pitzler, C., Wirtz, G., Vojcic, L. *et al.* (2014) *Chem. Biol.*, **21**, 1733–1742. doi: 10.1016/j.chembiol.2014.10.018.

Porter, J.L., Rusli, R.A. and Ollis, D.L. (2016) *Chembiochem*, **17**, 197–203. doi: 10.1002/cbic.201500280.

Puri, V., Streaker, E., Prabakaran, P. *et al.* (2013) *MAbs*, **5**, 533–539. doi: 10.4161/mabs.25211.

Renata, H., Wang, Z.J. and Arnold, F.H. (2015) *Angew. Chem. Int. Ed.*, **54**, 3351–3367. doi: 10.1002/anie.201409470.

Rhiel, L., Krah, S., Günther, R. *et al.* (2014) *PloS One*, **9**, e114887. doi: 10.1371/journal.pone.0114887.

Salaheddin, C., Spadiut, O., Ludwig, R. *et al.* (2009) *Biotechnol. J.*, **4**, 535–543. doi: 10.1002/biot.200800265.

Smith, G.P. and Petrenko, V.A. (1997) *Chem. Rev.*, **97**, 391–410. doi: 10.1021/cr960065d.

Spadiut, O., Radakovits, K., Pisanelli, I. *et al.* (2009) *Biotechnol. J.*, **4**, 525–534. doi: 10.1002/biot.200800260.

Tan, T.C., Kracher, D., Gandini, R. *et al.* (2015) *Nat. Commun.*, **6**, 7542. doi: 10.1038/ncomms8542.

Tanaka, T., Izawa, S. and Inoue, Y. (2005) *J. Biol. Chem.*, **280**, 42078–42087. doi: 10.1074/jbc.M508622200.

Tasca, F., Timur, S., Ludwig, R. *et al.* (2007) *Electroanalysis.*, **19**, 294–302. doi: 10.1002/elan.200603740.

Truppo, M.D. (2017) *ACS Med. Chem. Lett.*, **8**, 476–480. doi: 10.1021/acsmedchemlett.7b00114.

Vanella, R., Bazin, A., Ta, D.T. *et al.* (2019a) *Chem. Mater.*, **31**, 1899–1907. doi: 10.1021/acs.chemmater.8b04348.

Vanella, R., Ta, D.T. and Nash, M.A. (2019b) *Biotechnol. Bioeng.*, **116**, 1878–1886. doi: 10.1002/bit.27002.

Zámocký, M., Schümann, C., Sygmund, C. *et al.* (2008) *Protein Expr. Purif.*, **59**, 258–265. doi: 10.1016/j.pep.2008.02.007.

Zhu, B., Mizoguchi, T., Kojima, T. and Nakano, H. (2015) *PLoS One*, 10. doi: 10.1371/journal.pone.0127479.